Talanta 99 (2012) 394–403

Contents lists available at SciVerse ScienceDirect

Talanta

journal homepage: www.elsevier.com/locate/talanta

# Modification of coral-like $SnO_2$ nanostructures with dense $TiO_2$ nanoparticles for a self-cleaning gas sensor

Yuteng Wan [a,b], Jinyun Liu [a,*], Xiangqian Fu [a,b], Xiaoman Zhang [a,b], Fanli Meng [a], Xinyao Yu [a], Zhen Jin [a], Lingtao Kong [a], Jinhuai Liu [a,*]

[a] Research Center for Biomimetic Functional Materials and Sensing Devices, Institute of Intelligent Machines, Chinese Academy of Sciences, Hefei 230031, PR China
[b] Department of Materials Science and Engineering, University of Science and Technology of China, Hefei 230026, PR China

ARTICLE INFO

*Article history:*
Received 9 February 2012
Received in revised form
27 May 2012
Accepted 31 May 2012
Available online 16 June 2012

*Keywords:*
Nanostructure
Gas sensor
Environmental monitoring
Self-cleaning
Stability

ABSTRACT

A coral-like $SnO_2$ nanostructure densely-modified with $TiO_2$ nanoparticles was reported for developing a self-cleaning gas sensor. The density of the $TiO_2$ nanoparticles in the $TiO_2/SnO_2$ nanocomposites can be greatly improved via a plasma-based modification (PM) on $SnO_2$/carbonaceous precursors before introducing Ti sources. In gas-sensing measurements, benzene and toluene were employed as target analytes. The results show that the gas sensor based on the $TiO_2/SnO_2$ nanostructures with PM exhibits a remarkably improved stability after detecting for many cycles compared with the ones based on $TiO_2/SnO_2$ without PM and pure $SnO_2$ nanostructures. The mechanism for the stable performance has been demonstrated from the self-cleaning degradation of $TiO_2$ nanoparticles towards the adsorbed organic species. Furthermore, the recognizable ability towards targets was also investigated by using some algorithmic recognition methods including principal component analysis (PCA) and nonnegative matrix factorization (NMF). The fascinating gas-sensing properties including enhanced stability, sensitivity, and recognizable ability enable the presented $TiO_2/SnO_2$ nanocomposites to be a promising candidate for fabricating self-cleaning gas sensor which can be applied for detecting environmental gas contaminants.



## 1. Introduction

Nanomaterials have exhibited fascinating potential in a large variety of applications including electronic devices, energy storage, environmental purification, etc [1,2]. Among them, nanomaterial-based gas sensor which is a type of important electronic device applied in industrial production and our daily life has received broad attention. During the past few years, many efforts have been contributed to the synthesis of gas-sensing nanomaterials, the sensing mechanism of response, the fabrication of gas sensors based on single nanowire or nanotube, etc [3–5]. Most of the achievements pay attention to the improvement of sensitivity or selectivity. In contrast, the enhancement of stability of gas sensor which is also an important property for practical application has been rarely focused on.

$SnO_2$ is a representative n-type semiconductor with a wide band gap of 3.6 eV at room temperature. It has been widely used as a building block in sensors, lithium-ion batteries, solar-cells, and so on. In recent years, $SnO_2$ nanostructures with various morphologies have been developed to fabricate gas sensors for detecting a large range of analytes, e.g., CO, $H_2$, ethanol, and acetone [6–8]. However, as we know, the sensing mechanism of $SnO_2$ towards gases can be ascribed to the surface contact reactions. In air surroundings, $O_2$ is adsorbed on the surface of $SnO_2$ materials. It will capture and react with electrons from $SnO_2$ to produce negative oxygen species including $O^{2-}$, $O^-$, and $O_2^-$ [9,10], resulting in a high resistance in air. It is similar to some other semiconductors like $Fe_2O_3$ [11]. When the $SnO_2$-based sensor is exposed to gas analyte which is a oxidative or a reductive gas, some chemical reactions between negative oxygen species and gas molecules will take place, leading to the release of electrons back to $SnO_2$ and thereby changing the resistance. During such a gas-sensing process, some gas species especially the organic molecules which are not desorbed completely after gas-sensing reactions, would be adsorbed and remained on the surface of $SnO_2$. It will restrict $SnO_2$ materials to contact gas analyte in further detection. In this condition, the sensing performance of the gas sensor will be decayed gradually. So, it would be an effective strategy to improve the stability of gas sensor by removing the remained molecules from the surface of sensing materials.

In order to address this challenge, herein, we report the modification of $SnO_2$ nanostructures with dense $TiO_2$ nanoparticles to develop a self-cleaning gas sensor, as shown in Scheme 1.

* Corresponding authors. Tel.: +86 551 5591142; fax: +86 551 5592420.
*E-mail addresses:* jyliu@iim.ac.cn (J. Liu), jhliu@iim.ac.cn (J. Liu).

0039-9140/$ - see front matter © 2012 Elsevier B.V. All rights reserved.
http://dx.doi.org/10.1016/j.talanta.2012.05.070

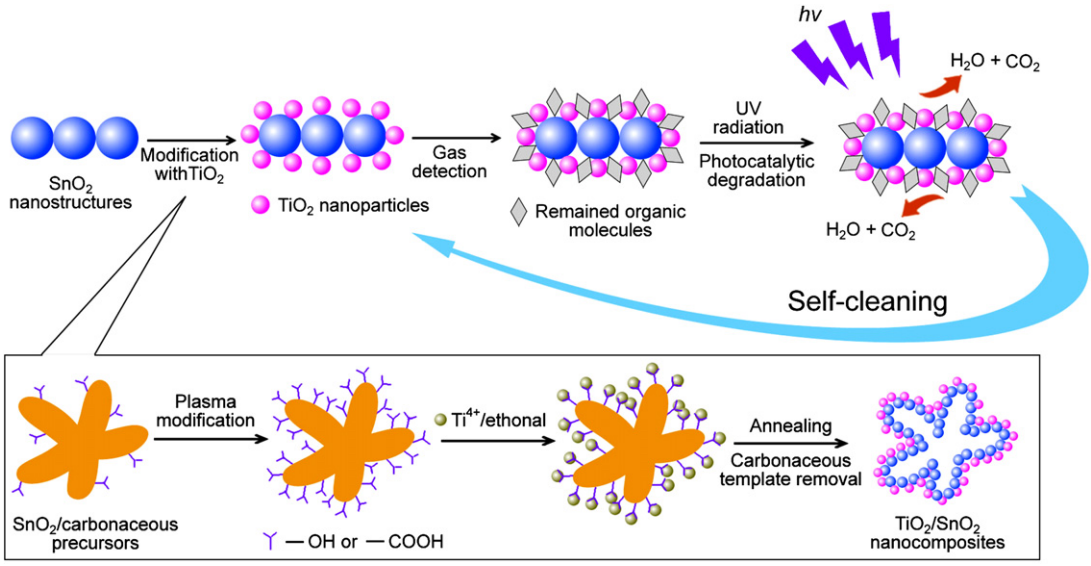


**Scheme 1.** Illustration of the modifying process of coral-like $SnO_2$ nanostructures and the self-cleaning mechanism of the $TiO_2/SnO_2$ nanocomposites.

In such a $TiO_2/SnO_2$ nanocomposite, the photocatalysis of $TiO_2$ nanoparticles is used to degrade the adsorbed organic molecules remained during gas-sensing process. As we know, under a condition of ultraviolet (UV) radiation, the remained organic molecules can be photocatalytically degraded by $TiO_2$ [12]. So, $TiO_2$ can keep the sensing layer fresh for further gas-sensing detections. On the basis of the removal of adsorbed organic contaminants on the surface of sensing materials, it would enable the gas sensor based on the $TiO_2/SnO_2$ nanocomposites to exhibit a fascinating self-cleaning performance. In recent years, the cooperation between $TiO_2$ and some semiconductors have been of great interests, such as $TiO_2$/ZnO and $TiO_2$/CuO [13,14]. However, as for the $TiO_2/SnO_2$ composites, firstly, most of the efforts are focused on the thin films instead of nanostructures [15–17]. It is hard to effectively show the advantages of $TiO_2$ due to the cover of most active sites located at the inside layer of the film. Secondly, as for some conventional $TiO_2$-modified $SnO_2$ nanostructures, the quantity of $TiO_2$ is relatively low which leads to a limited performance of $TiO_2$. Moreover, most reports focused on the photocatalytical properties of the nanocomposites [18–20]. In our investigation, a plasma-assisted approach was employed for modifying $TiO_2$ nanoparticles onto $SnO_2$ nanostructures in a large density (Scheme 1). The plasma treatment is a solvent-free process which can be used for functionalizing many materials [21,22]. We have found that the density of some functional groups (e.g., –OH and –COOH) can be greatly improved on the surface of some materials treated by plasma [23–25]. Previously, we have developed a coral-like $SnO_2$/carbonaceous nanostructure, which is found to possess a good diffusing ability in dye-sensitized solar cell application [26]. Such a special structure would also be an advantage to achieve improved contact between $SnO_2$ and gas analytes. So, it is employed to study the modification with $TiO_2$ nanoparticles for developing a special gas sensor which possesses a self-cleaning property. In gas-sensing measurements, benzene and toluene were used as target gases. Both of them are typical volatile organic compounds which are seriously harmful to our health. Besides, desorption of them and their mid-products (such as some small organic species) formed during gas-sensing process is difficult, resulting in great difficulty to develop long-term stable gas sensors of them. The self-cleaning gas sensor presented here would be a potential candidate for detecting benzene and toluene with good stability. In addition, the sensitivity, response and recovery times, and the recognizable ability towards targets based on some identifying methods including principal component analysis (PCA) and nonnegative matrix factorization (NMF) were also investigated.

## 2. Experimental section

### 2.1. Preparation of coral-like $SnO_2$/carbonaceous precursors

All chemicals were analytical grade and used without further purification as purchased from Shanghai Chemical Reagents Company. The coral-like $SnO_2$/carbonaceous precursors were synthesized through a hydrothermal method, as reported previously [26]. Firstly, 10 mmol $SnCl_4 \cdot 5H_2O$ and 20 mmol sucrose were dissolved into de-ionized water to form a 35 mL solution by constant stirring. Secondly, the solution was transferred into a Teflon-lined stainless steel autoclave with a capacity of 50 mL. The autoclave was sealed and heated in an oven at 170 °C for 6 h. Thirdly, after the reaction was completed, the brown precipitates were collected by centrifugation and washed for several times with ethanol and de-ionized water alternately. Finally, they were dried in a vacuum oven at 60 °C for 6 h.

### 2.2. Plasma-based modification (PM) of $SnO_2$/carbonaceous precursors and the preparation of $TiO_2/SnO_2$ nanocomposites

The as-prepared $SnO_2$/carbonaceous precursors were treated by an inductively coupled plasma (ICP) apparatus, which consisted of a three-neck glass bottle and several cycles of copper wire wrapped around the glass bottle (Fig. S1 of Supporting information). The inside diameter and length of the bottle are 5 and 20 cm, respectively. The radio frequency (RF) power at a frequency of 13.5 MHz was fed to the copper wire. In the plasma treatment, 2 g $SnO_2$/carbonaceous precursors were put into the flask and evacuated to ca. 10 Pa. The system was flushed with argon gas flow, and then evacuated back to 10 Pa. After three times of flushing and evacuating processes, the $SnO_2$/carbonaceous precursors were treated by argon/oxygen plasma at a flow ratio of 5:1 under constant stirring for 30 min. After that, the plasma-treated samples were dried in a vacuum oven at 60 °C for further use.

As for the preparation of the $TiO_2$ nanoparticles-modified $SnO_2$ nanostructures, a adsorbing process followed by an annealing

treatment were carried out, which can also be illustrated in Scheme 1. For example, as for the preparation of the $TiO_2/SnO_2$ nanostructures with PM, firstly, the plasma-treated $SnO_2$/carbonaceous precursors (0.2 g) were ultrasonically dispersed in 10 mL Tetra-n-butyl Titanate solution (0.1 M) which was obtained by dissolving a certain amount of $C_{16}H_{36}O_4Ti$ into ethanol. And then, the mixed solution was left for 24 h at room temperature statically. Secondly, after several cycles of washing and centrifugation, the samples were dried in an oven at 60 °C for 6 h. At last, the samples were annealed in a furnace under a program-controlled heating condition (from room temperature to 550 °C at a rate of 10 °C $min^{-1}$, and keeping at 550 °C for 1 h) in air surroundings. For the comparison of gas-sensing properties, the coral-like $TiO_2/SnO_2$ nanostructures without PM were prepared based on the $SnO_2$/carbonaceous precursors which have not been treated by plasma. The pure $SnO_2$ were prepared through the same hydrothermal and annealing processes.

### 2.3. Characterization

The as-obtained samples were characterized by using a Philips X' Pert Pro X-ray diffractometer (XRD) with Cu Kα radiation (1.5418 Å), a FEI Sirion 200 field emission scanning electronic microscopy (FESEM), and a JEOL JEM-2010 transmission electron microscopy (TEM) equipped with an Oxford INCA energy dispersive X-ray analysis (EDX) at an accelerating voltage of 200 kV. The diffraction peaks of crystalline phases were compared with the patterns in the Joint Committee on Powder Diffraction Standards (JCPDS). The elemental mappings and the line scans were performed in the high-angle annular dark-field (HAADF) mode on the same TEM. The composition analysis of the samples was carried out on an ESCALab MK II X-ray photoelectron spectrometer (XPS) using monochromatized Al Kα X-ray beams as excitation source. Binding energies were calibrated relative to the C 1s peak at 284.6 eV.

### 2.4. Fabrication of gas sensor and gas-sensing measurement

The structure of the gas sensor is shown in Fig. 1. As for the fabrication of it, firstly, the as-prepared nanostructures were dispersed in absolute alcohol and rotatingly-coated onto the surface of $SiO_2$ substrate covered with comb-like gold electrodes and a $RuO_2$ layer as heater on the back side. Secondly, the sensors were dried in an oven at 80 °C. In order to enhance the repeatability of gas-sensing performance, the as-fabricated gas sensors were aged for 48 h before detection.

In gas-sensing measurement, it was carried out by using a computer-controlled gas-detecting system in which a Keithley 6487 picoameter/voltage sourcemeter was employed as both current recorder and power source. All gas-sensing measurements were carried out at the same working temperature of gas sensors (200 °C) and humidity of ambient atmosphere (30% RH). It should be indicated that the relative humidity was the value measure in the mixture of pure air and target gases at room temperature. Benzene and toluene at a series of concentrations ranging from 50 to 200 ppm were employed as target gases. Besides, for the investigation of recognizable ability of the gas sensor towards targets, some other gases which were used as the interference gases, including 100 ppm aether, acetone, formaldehyde, and hexane, accordingly, were also detected at the same working condition of the sensor. The recognizable ability towards targets was investigated by using two algorithmic recognition methods, i.e. principal component analysis (PCA) and nonnegative matrix factorization (NMF). PCA is an efficient method to extract feature sets by creating a feature space [27,28]. PCA has short computation time which is an important advantage of it. NMF is a bilinear model used to factorize a multivariate dataset into two matrices including G and F which are called factor scores and factor loadings matrices, respectively, as shown in Eq. (1) [29]. Herein, NMF was also used to extract features from real-time gas-sensing curves.

$$X = GF + E \tag{1}$$

$$S = \frac{R_{air}}{R_{gas}} = \left(\frac{I_{gas}}{I_{air}}\right)_V \tag{2}$$

The response of sensor is defined as Eq. (1), where $R_{air}$ is the resistance of sensor in pure air while $R_{gas}$ is that in the gas mixture of pure air and target gas. By following Ohm's Law, $S$ can also be expressed by the currents in pure air ($I_{air}$) and gas mixture ($I_{gas}$) under a constant measuring voltage. Moreover, the response and recovery times are determined by the times for gas sensor to achieve 90% of the total resistance change in the cases of gas injection and discharge, respectively.

## 3. Results and discussion

### 3.1. Morphology, structure and composition of nanostructures

The XRD patterns of the pure sample and the ones modified by $TiO_2$ with or without PM are shown in Fig. 2. As shown in Fig. 2A, all the diffraction peaks can be readily indexed to the rutile structure of $SnO_2$ with lattice constants of $a=0.4737$ nm and $c=0.3186$ nm, which are in good agreement with the values in literature (JCPDS no. 41-1445). Seen from Fig. 2B and C, the anatase phase of $TiO_2$ can be observed (JCPDS no. 84-1285). Especially seen from the XRD pattern of the sample modified by

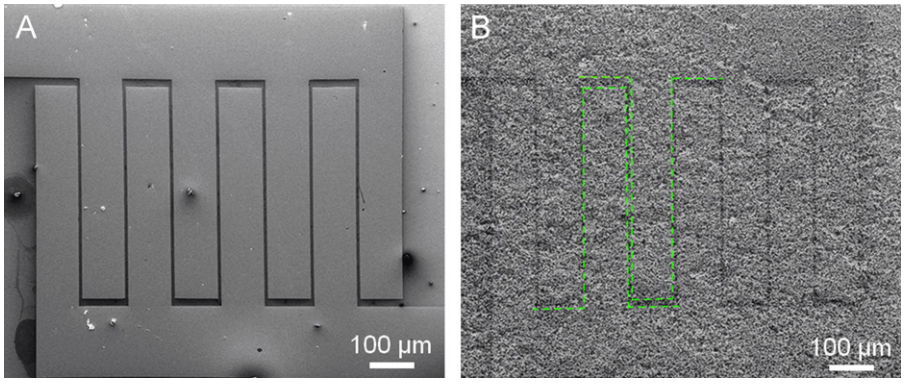


**Fig. 1.** FESEM images of the structures of (A) blank sensor and (B) nanostructures-based gas sensor. The dash lines in (B) indicate the gold electrodes covered by $SnO_2$ nanostructures.

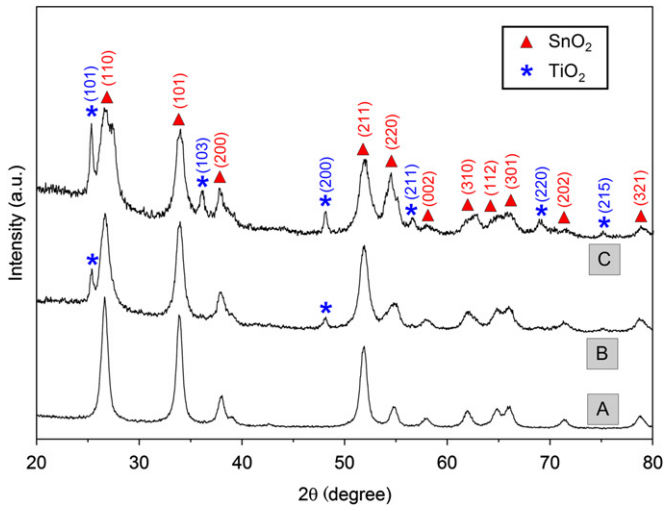


**Fig. 2.** XRD patterns of (A) pure $SnO_2$, (B) $TiO_2/SnO_2$ composites without PM, and (C) $TiO_2/SnO_2$ composites with PM.

$TiO_2$ with PM (Fig. 2C), the diffraction peaks of $TiO_2$ structure are remarkably obvious than the one without PM (Fig. 2B). For example, the peaks ($2\theta$) at ca. 37.0°, 55.1°, 69.9°, and 74.9° can be assigned to the (103), (211), (2 2 0), and (215) crystalline planes of $TiO_2$ crystals, respectively. It is indicated that the amount of $TiO_2$ in the $TiO_2/SnO_2$ composites with PM is greatly larger than the one without PM. In other words, the density of $TiO_2$ can be effectively improved by the plasma-based treatment towards the $SnO_2$/carbonaceous precursors previously. The further supports by using XPS analysis and elemental mappings will be show below.

In addition, it can be found that the full width at half maximum of the diffraction peaks in Fig. 2B and C is obviously broader than that of Fig. 2A by following a sequence (from large to small) of $TiO_2/SnO_2$ with PM, $TiO_2/SnO_2$ without PM, and pure $SnO_2$. It is indicated that the average particle size of $TiO_2/SnO_2$ with PM is the smallest among the three samples by following the Scherrer formula [30]. The calculated values corresponding to them are ca. 10.3, 14.4, and 17.6 nm, respectively. The mechanism for such a reduced particle size can be explained by some reports on doping [31–33]. In a doped crystal, the motion of crystallites is restricted due to the interaction on the boundaries between host and dopants, resulting in the disadvantage of further growth of crystalline grains [34]. It should be indicated that there is no obvious newly-formed phases that can be observed in the XRD patterns. It would be ascribed to the relatively low amount of the doped structure, which leads to a difficulty for XRD characterization. However, the annealing process at about 550 °C for 1 h was performed after the adsorption of $Ti^{4+}$. It would result in a combination and doping effect during the annealing process in which the crystallinity was achieved. In our study, the remarkably reduced particle size indicates that it is an effective method for doping $TiO_2$ to $SnO_2$ using plasma treatment towards $SnO_2$/carbonaceous precursors. Besides, the small particle size would achieve improved gas-sensing properties compared with the large one because of the enlarged surface area and the enhanced adsorbing capability towards analytes.

Fig. 3 shows the FESEM and TEM observations on the plasma-treated $SnO_2$/carbonaceous precursors, pure $SnO_2$, $TiO_2/SnO_2$ without PM, and $TiO_2/SnO_2$ nanostructures with PM. As can be seen from the $SnO_2$/carbonaceous precursors after PM (Fig. 3A), the morphology keeps a coral-like profile without destroying the structure. It should be indicated that the removal of carbonaceous components in the $SnO_2$/carbonaceous precursors by the annealing process can be supported by the comparison on the TEM images between the pure $SnO_2$ nanostructures and them (Fig. S2 of Supporting information). In Fig. 3C–E, the $TiO_2/SnO_2$ nanostructures without PM are presented, which is close to the pure $SnO_2$ (Fig. 3B). The porous and hollow structure can be clearly observed. In contrast, as shown in Fig. 3F–I, the surface of $TiO_2/SnO_2$ nanostructures with PM becomes remarkably rough compared with the pure $SnO_2$ and the $TiO_2/SnO_2$ without PM. It can be found that there are many particles on the surface of each antenna, exhibiting a highly-dense modification of the $TiO_2$ on $SnO_2$. It should be indicated that there are no obvious $TiO_2$ nanoparticles which can be observed clearly in the high-magnification TEM image (Fig. 3I). It would be caused by the overlap among nanoparticles in such a high density.

The composition of the as-prepared samples was investigated by XPS analysis, as shown in Fig. 4. As indicated in Fig. 4A, the component of Ti can be detected in the $TiO_2/SnO_2$ with and without PM. Especially seen from the high-resolution XPS spectra of Ti 2p region (Fig. 4B), it can be found that the intensity and area of the XPS peak of $TiO_2/SnO_2$ nanostructures with PM are obviously larger than the ones of $TiO_2/SnO_2$ without PM. It is indicated that the amount of Ti in the $TiO_2/SnO_2$ with PM is more than the one in the $TiO_2/SnO_2$ without PM, further supporting the enhanced modification of $TiO_2$ to $SnO_2$ by the plasma-assisted treatment. The quantitative results of elements corresponding to the XPS spectra are shown in Table 1. It can be found that the molar ratios of Ti to Sn in the $TiO_2/SnO_2$ with and without PM are ca. 0.45:1 and 0.14:1, respectively. In other words, the amount of Ti in $TiO_2/SnO_2$ nanostructures with PM is about 3 times to the Ti in $TiO_2/SnO_2$ without PM. Moreover, it can also be found that the ratio of O 1s decreases accompanying with the increase of C 1s correspondingly. It can be ascribed to the influence of organic species adsorbed on the surface of nanostructures. In our study, the plasma-assisted treatment towards the $SnO_2$/carbonaceous precursors was followed by an adsorbing process of $Ti^{4+}$ ions and an annealing oxidization procedure. So, the change of the percentage of O and C elements in the final products would be more likely caused by the adsorbed organic species rather than the plasma treatment. The elemental distribution of the $TiO_2/SnO_2$ nanostructures with PM was further studied by elemental mappings of Sn Lα1 and Ti Kα1, as shown in Fig. 5. The profile of Ti Kα1 is very close to that of Sn Lα1. It indicates that the Ti element distributes uniformly and densely although the coral-like structure. Besides, seen from the compositional scanline (Fig. 5D), a valley-type shape is clearly presented, indicating that the nanostructure is hollow. Besides, the similar profile of Sn and Ti scanlines further confirm that the Ti element distributes along the Sn element uniformly. The quantitative molar ratio of Ti to Sn is ca. 0.41:1, which is close to the XPS results demonstrated above.

### 3.2. Gas-sensing properties

Fig. 6 shows the gas-sensing responses of the sensors based on pure $SnO_2$ nanostructures, $TiO_2/SnO_2$ nanocomposites with or without PM towards benzene and toluene at a series of concentrations. As indicated in Fig. 6A, when the gas analyte was injected into the test chamber, the current of sensor increased rapidly, indicating that the coral-like $TiO_2/SnO_2$ nanostructures with PM is sensitive to benzene. It can be well supported by the calculated values of response, the response and recovery times, as shown in Fig. 6B and C. Seen from Fig. 6B, the responses of $TiO_2/SnO_2$ nanostructures with PM are remarkably higher than the ones of pure $SnO_2$ and $TiO_2/SnO_2$ without PM. For example, the responses to 100 ppm benzene of pure $SnO_2$, $TiO_2/SnO_2$ without PM, and $TiO_2/SnO_2$ with PM are ca. 3, 4, and 9, respectively. The improved response can be ascribed to the modification of $SnO_2$

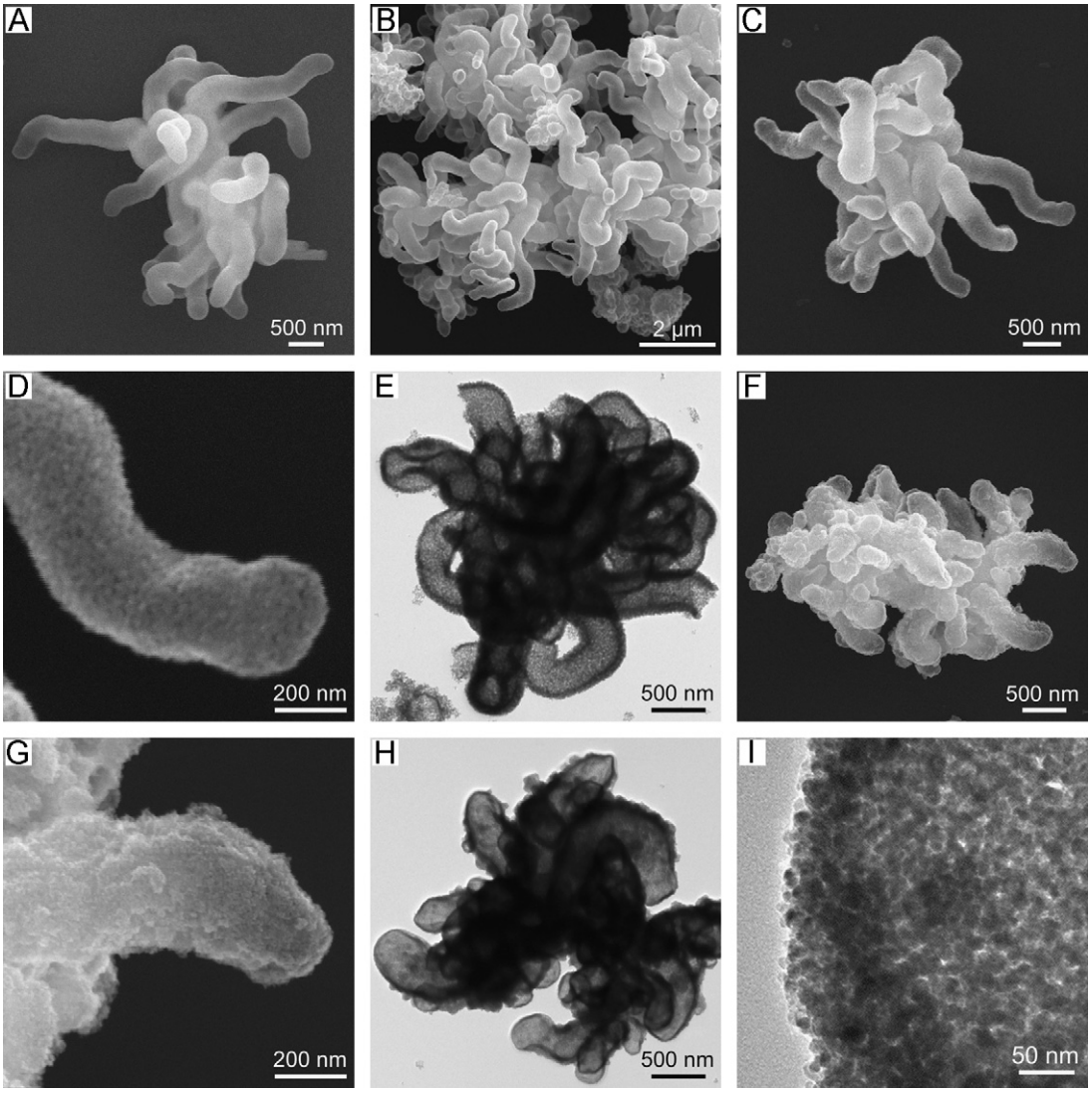


**Fig. 3.** FESEM images of (A) $SnO_2$/carbonaceous precursors, (B) pure $SnO_2$, (C) and (D) $TiO_2/SnO_2$ without PM, and (F) and (G) $TiO_2/SnO_2$ nanostructures with PM; TEM images of (E) $TiO_2/SnO_2$ without PM, and (H) and (I) $TiO_2/SnO_2$ nanostructures with PM.

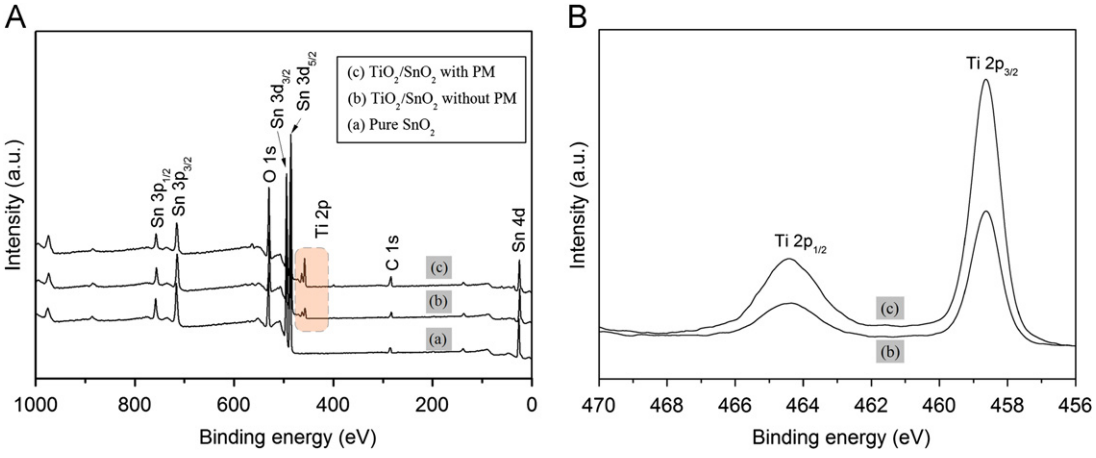


**Fig. 4.** (A) XPS survey spectra of (a) pure $SnO_2$ nanostructures, (b) $TiO_2/SnO_2$ without PM, and (c) $TiO_2/SnO_2$ with PM; (B) the corresponding high-resolution spectra of Ti 2p region of (b) and (c).

with dense $TiO_2$ nanoparticles. Firstly, as for the aspect outside the $SnO_2$ crystals, there are some $TiO_2$ enriched on the surface too, as observed by FESEM and TEM. In this condition, by following the theoretical calculation studied by Hahn et al. [35], a $TiO_2/SnO_2$ system with Ti elements distributed on the surface (surface enrichment) had low surface energies and thus were

thermodynamically favorable because of the lower energy necessary to break the Ti–O bonds than Sn–O ones. They also demonstrated that it would facilitate the breaking of Sn–O bonds in the vicinity of Ti atoms. Secondly, the particle size of $SnO_2$ is reduced by the modification with $TiO_2$, which can be supported by the XRD patterns as demonstrated above. On one hand, the decreased particle size would enlarge the surface area of nanostructures, which is advantageous for gas adsorption. On the other hand, by following the theoretical gas-sensing models proposed by Xu and co-workers [36], the smaller the nanoparticle is, the higher the gas-sensing response will be. In the models mentioned above, when the nanostructures with large particle size ($D$), the gas response is influenced by grain boundaries. As $D$ is comparable to the two-fold thickness of a charge depletion layer ($2L$), the gas response is a neck-controlled model. While $D$ is less than $2L$, the depletion region extends throughout the whole nanoparticle and the crystallites are almost fully-depleted of charge carriers. Correspondingly, the resistance of sensor is dominated by the particles themselves to form a particle size-controlling model. In this condition, the response will be improved significantly. In our study, the average particle size of the $TiO_2/SnO_2$ with PM (ca. 10.3 nm) is close to that value. It would be the theoretical mechanism for such a remarkable enhancement of gas-sensing response. Additionally, $TiO_2$ is also a typical sensitive semiconductor. It would also play an important role in gas-sensing processes.

**Table 1**
Atomic percentages of the pure $SnO_2$ nanostructures, $TiO_2/SnO_2$ without PM, and $TiO_2/SnO_2$ with PM.

| | Atomic percentage (at%) | | | |
|---|---|---|---|---|
| | Sn 3d | Ti 2p | O 1s | C 1s |
| Pure $SnO_2$ | 22.03 | – | 61.67 | 16.30 |
| $TiO_2/SnO_2$ without PM | 23.63 | 3.23 | 58.11 | 15.03 |
| $TiO_2/SnO_2$ with PM | 20.55 | 9.15 | 52.29 | 19.01 |

In contrast, as for the $TiO_2/SnO_2$ without PM, the improvement of response is not so obvious compared with the $TiO_2/SnO_2$ with PM. In $TiO_2/SnO_2$ without PM, the modification is not so effective and dense, which makes it hard to exhibit the advantages of composite. In Fig. 6C, it can be found that both the response and the recovery times of $TiO_2/SnO_2$ nanostructures with PM are the shortest among the three samples. Seen from Fig. 6D–F, the gas-sensing properties towards toluene show a trend similar to that of benzene. The $TiO_2/SnO_2$ nanostructures with PM also exhibit an obviously improved sensing performance towards toluene compared with pure $SnO_2$ and $TiO_2/SnO_2$ without PM.

In order to investigate the self-cleaning performance of the as-prepared nanostructures, a series of experiments with 5 detecting cycles were carried out, as shown in Fig. 7. It should be indicated that it is an alternative for gas detection and UV radiation treatment. In other words, after the detection towards gases from 50 to 200 ppm, all gas sensors were radiated under UV light for 30 min. By following the radiation, sensors were closed in a box and put for half a month. Subsequently, the next gas-detecting cycle was performed. Seen from Fig. 7A, it can be found that the gas-sensing responses of different detecting cycles are close to each other, indicating that the $TiO_2/SnO_2$ nanostructures with PM exhibit a stable performance after detecting for many times. It can be ascribed to the photocatalytic degradation of $TiO_2$ components in the $TiO_2/SnO_2$ nanocomposites. After a cycle of gas-sensing detection, there would be numerous remained organic species adsorbed on the surface of sensing layer. By following an UV radiation treatment, the organic species mentioned above can be degraded photocatalytically. It will lead to the formation of a

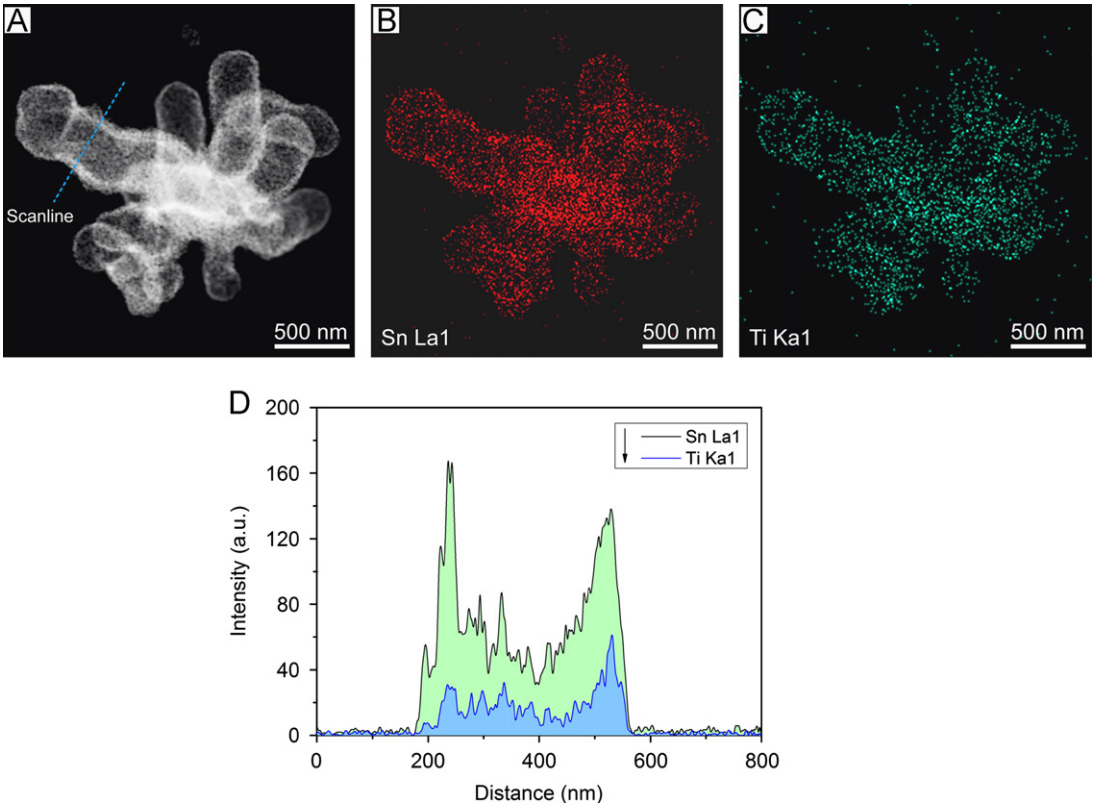


**Fig. 5.** (A) HAADF–TEM image of the $TiO_2/SnO_2$ nanostructures with PM; (B) elemental mapping of Sn Lα1; (C) elemental mapping of Ti Kα1; and (D) the compositional lines of Sn and Ti recorded along the scanline marked in (A).

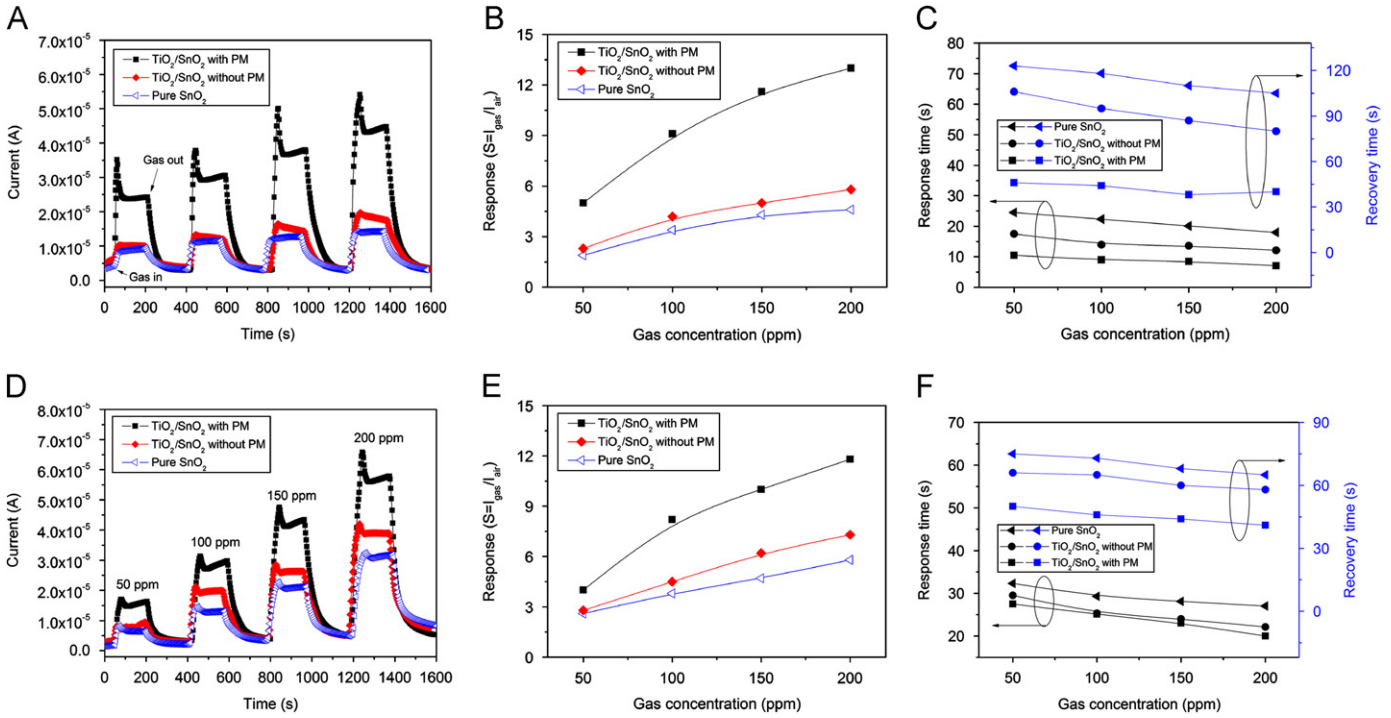


**Fig. 6.** (A) Real-time gas-sensing curves towards benzene of the sensors based on pure $SnO_2$ nanostructures, $TiO_2/SnO_2$ nanostructures with or without PM; (B) the values of response and (C) the response and recovery times calculated from (A). Correspondingly, (D) is the real-time gas-sensing curves towards toluene, (E) is the calculated values of response, and (F) is the response and recovery times.

clean sensing surface again, showing a fascinating self-cleaning property of the presented gas sensor. In contrast, the gas-sensing responses of the $TiO_2/SnO_2$ nanostructures without PM and the pure $SnO_2$ decrease gradually depending on the increase of detecting cycles, as shown in Fig. 7B and C. As for the $TiO_2/SnO_2$ nanostructures without PM, the density of the $TiO_2$ nanoparticles in the $TiO_2/SnO_2$ nanocomposites is relatively low, which makes it hard to exhibit a good degrading performance towards the remained organic species on sensing materials.

Taking the detection of 100 ppm benzene as an example (Fig. 7D), the gas-sensing properties of the $TiO_2/SnO_2$ nanostructures with PM remain stable. Under the same working conditions, the decay of the gas-sensing responses of $TiO_2/SnO_2$ nanostructures without PM and pure $SnO_2$ are serious, especially for the pure one. It should be indicated that the change of absolute response value seems to be not so great for the $TiO_2/SnO_2$ nanostructures without PM and pure $SnO_2$. However, the percentage of the change of response is remarkable. For instance, from the first to the fifth cycles, the response of the $TiO_2/SnO_2$ nanostructures with PM changes from 9.6 to 9.0, while that is from 4.4 to 3.5 for the $TiO_2/SnO_2$ without PM, and that is from 4.0 to 2.0 for the pure $SnO_2$ nanostructures. The changes of absolute response values of $TiO_2/SnO_2$ nanostructures with PM, $TiO_2/SnO_2$ without PM, and pure $SnO_2$ are 0.6, 0.9, and 2.0, respectively, which are close to each other. Nevertheless, the corresponding changes of the percentages, i.e. $(S_0-S)/S_0$, are ca. 6.3%, 20.5%, and 50%, respectively. It clearly reveals that the gas-sensing stability of the $TiO_2/SnO_2$ nanostructures with PM is significantly improved compared with the $TiO_2/SnO_2$ without PM and the pure $SnO_2$. It can be ascribed to the high density of $TiO_2$ nanoparticles in the $TiO_2/SnO_2$ nanocomposites with PM. The good stability can also be well supported by the detection towards toluene, as shown in Fig. 7E–H. As can be seen, it shows a similar trend of stability during a series of detection towards toluene. From the first to the fifth detecting cycles, the percentage changes of the response of $TiO_2/SnO_2$ with PM, $TiO_2/SnO_2$ without PM, and pure $SnO_2$ nanostructures, are ca. 4.6%, 19.4%, and 32.1%, respectively. The same as the detection of benzene, the $TiO_2/SnO_2$ nanostructures with PM exhibit a remarkably improved gas-sensing stability towards toluene compared with the $TiO_2/SnO_2$ without PM and the pure $SnO_2$ nanostructures. Furthermore, under a condition without UV-radiation, the gas-sensing performance of the three sensors was also investigated. It should be indicated that all the sensors were measured for the three cycles using benzene and toluene as the target gases. The real-time gas-sensing curves are shown in Fig. S3 of Supporting information, while the correspondingly calculated responses are shown in Fig. S4 of Supporting information. It can be found that the trends of the response change are close to the ones under UV radiation. The $TiO_2/SnO_2$ nanostructures with PM show relatively stable performance compared with the $TiO_2/SnO_2$ without PM and the pure $SnO_2$. However, even the $TiO_2/SnO_2$ nanostructures with PM, there are some decay which can be observed, indicating that the UV-radiation condition would be essential to achieve a good self-cleaning degradation of $TiO_2$. It is expected that the visible light degradation of $TiO_2$ in $TiO_2/SnO_2$ nanostructures can be potentially improved by using some doping process which is greatly valuable for further study.

In addition, besides to the gas-sensing stability and sensitivity, the selectivity of the gas sensors is also an important characteristic for practical applications. As we know, $SnO_2$ is sensitive to a large variety of gases [37]. In our study, two widely-used algorithmic recognition methods including PCA and NMF were employed to investigate the recognizability of the $TiO_2/SnO_2$ nanostructures with PM towards different target gases. In gas-sensing measurements, aether, acetone, formaldehyde, and hexane at a concentration of 100 ppm were used as interference gases, respectively. The same as the detection towards benzene and toluene, each interference gas was detected for 4 times repeatedly. The real-time sensing responses are shown in Fig. S5 of Supporting information. On the basis of these real-time curves, the PCA and NMF analysis were performed, respectively, as shown

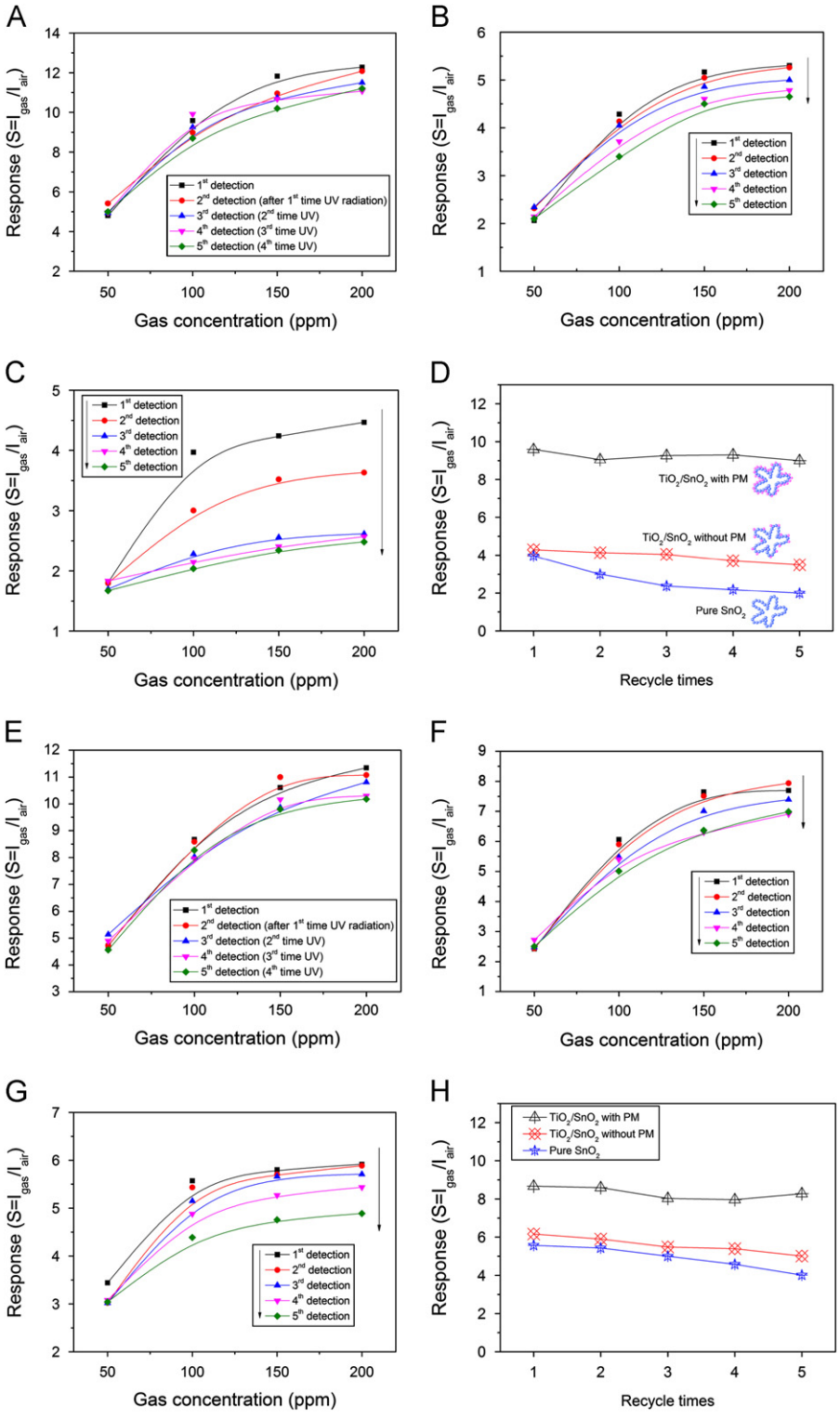


**Fig. 7.** Gas-sensing responses of (A) $TiO_2/SnO_2$ nanostructures with PM, (B) $TiO_2/SnO_2$ without PM, and (C) pure $SnO_2$ towards 50–200 ppm benzene in every detecting cycle; (D) shows the values of the response towards 100 ppm benzene; correspondingly, (E), (F), (G), and (H) are gas-sensing results towards toluene.

in Fig. 8. Seen from the three-dimensional PCA classification towards each gases (Fig. 8A), it can be clearly observed that the characters extracted from the gas-sensing curves of each gas located at a specific region are different from other gases. It is indicated that the target gases, even though the interference gases themselves, can be clearly recognized by the sensor based on the $TiO_2/SnO_2$ nanocomposites combining with a PCA method. The variances explained in PC1, PC2, and PC3 are 94.4%, 3.2%, and 1.36%, respectively. For further investigating the general application of the presented gas sensor, NMF as another algorithmic recognition method was also used to identify each gas (Fig. 8B). It can also be found that not only benzene and toluene can be clearly recognized, but also the interference gases can be distinguished easily. Such a fascinating recognizable ability towards different gases would be ascribed to the special sensing behaviors of the densely-modified nanocomposites with two

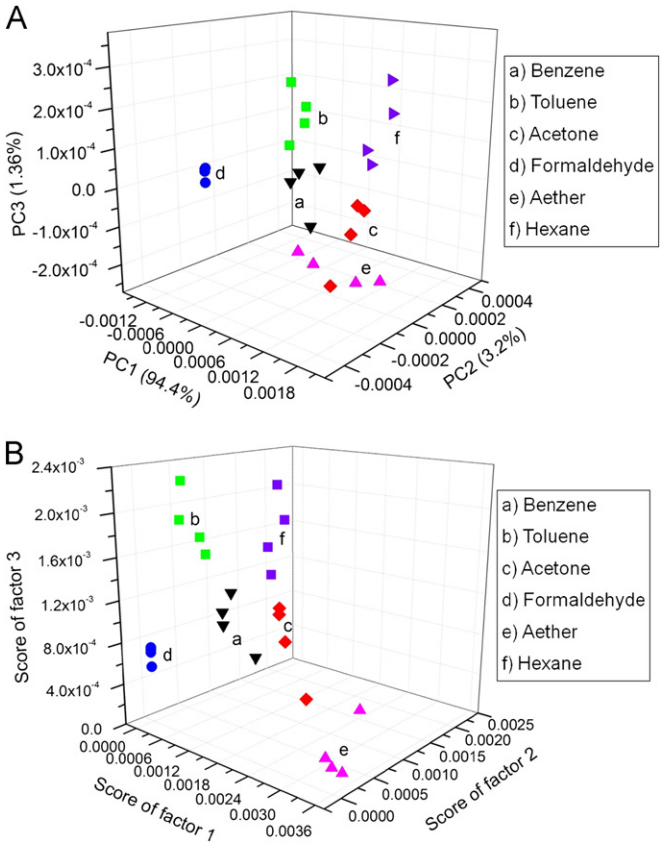


**Fig. 8.** The three-dimensional (A) PCA and (B) NMF analyzing results for the recognition of different gases.

semiconductors at a close energy bandgap. In addition, the coral-like morphology combining with porous and hollow structure would also play a significant role for influencing the gas adsorbing/desorbing processes, which enables the gas sensor possess specific sensing characters towards different gases. Of course, the detection towards real gas samples still needs to be further studied. As we know, the decorating materials would release some organic gas species, such as benzene, toluene, formaldehyde, etc. We found that the sensor based on the $TiO_2/SnO_2$ nanostructures with PM exhibited a response towards the real gas sample collected from a newly-decorated room. As for the classification towards the components in the gas sample, it is still not achieved simply by only one gas sensor. However, it can be expected that it could be achieved by using a sensor array combining with some identifying mathematic methods, which would be a fascinating direction for future investigation for practical applications.

## 4. Conclusions

In summary, a coral-like $SnO_2$ nanostructure modified with dense $TiO_2$ nanoparticles was prepared for the fabrication of a self-cleaning gas sensor. The density of $TiO_2$ nanoparticles in the $TiO_2/SnO_2$ nanocomposites can be greatly improved by a plasma-assisted modification on the $SnO_2$/carbonaceous precursors. It is found that the moral ratio of Ti to Sn in the $TiO_2/SnO_2$ nanostructures with PM is about 3-fold compared with the value in the $TiO_2/SnO_2$ without PM. On the basis of the photocatalytical degradation of $TiO_2$ nanoparticles under UV radiation, the $TiO_2/SnO_2$ nanostructures with PM exhibit a remarkably enhanced gas-sensing stability after detecting benzene and toluene for many cycles at a series of concentrations. After detecting 100 ppm benzene for 5 cycles, the decay percentages of gas-sensing responses of the $TiO_2/SnO_2$ with PM, the $TiO_2/SnO_2$ without PM, and the pure $SnO_2$ nanostructures are ca. 6.3%, 20.5%, and 50%, respectively. As for the toluene, the corresponding decay percentages are ca. 4.6%, 19.4%, and 32.1%, respectively. Moreover, the $TiO_2/SnO_2$ nanostructures with PM also show an improved sensitivity compared with the $TiO_2/SnO_2$ without PM and the pure $SnO_2$. At last, by using some algorithmic recognition methods including PCA and NMF, it is found that the target analytes, including benzene, toluene, and some interference gases such as aether, acetone, formaldehyde and hexane can be recognized clearly. Such a good performance on stability, sensitivity, and recognizable ability towards targets, indicates that the self-cleaning gas sensor based on the as-prepared coral-like $TiO_2/SnO_2$ nanocomposites could be promisingly applied for environmental gas monitoring.

## Acknowledgment

This work was financially supported by the "973" State Key Project of Fundamental Research for Nanoscience and Nanotechnology (no. 2011CB933700), the National Natural Science Foundation of China (nos. 51002157, 61071054, 21177131, and 61104205), and the One Hundred Person Project of the Chinese Academy of Sciences. Moreover, Prof. Ming Gong from University of Science and Technology of China was appreciated for his useful discussion on elemental mappings.

## Appendix A. Supporting information

Supplementary information associated with this article can be found in the online version, including the schematic diagram of the inductively coupled plasma instrument; TEM images of the $SnO_2$/carbonaceous precursors and pure $SnO_2$ nanostructures; real-time sensing curves of the sensors based on pure $SnO_2$ nanostructures, $TiO_2/SnO_2$ nanostructures with or without PM towards benzene and toluene without UV radiation; and the real-time sensing responses of the $TiO_2/SnO_2$ nanostructures with PM towards aether, acetone, formaldehyde, and hexane at a concentration of 100 ppm, respectively. http://dx.doi.org/10.1016/j.enpol.2011.12.024.

## References

[1] J.S. Jie, W.J. Zhang, I. Bello, C.S. Lee, S.T. Lee, Nano Today 5 (2010) 313–336.
[2] M.S. Anderew, S. Nie, Acc. Chem. Res. 43 (2010) 190–200.
[3] Y. Zhou, K.B. Zheng, J.D. Grunwaldt, T. Fox, L.L. Gu, X.L. Mo, G.R. Chen, G.R. Patzke, J. Phys. Chem. C 115 (2011) 1134–1142.
[4] M.W. Ahn, K.S. Park, J.H. Heo, J.G. Park, D.W. Kim, K.J. Choi, J.H. Lee, S.H. Hong, Appl. Phys. Lett. 93 (2008) 263103.
[5] K.J. Li, W.C. Wang, D.P. Cao, J. Phys. Chem. C 115 (2011) 12015–12022.
[6] P. Surachet, T. Suvit, M. Pongsri, C. Supab, M. Nikorn, W. Duangmanee, Curr. Appl. Phys. 11 (2011) 1368–1373.
[7] J.W. Gong, J.R. Sun, Q.F. Chen, Sens. Actuators B 130 (2008) 829–835.
[8] J. Huang, Q. Wan, Sensors 9 (2009) 9903–9924.
[9] X.J. Huang, F.L. Meng, Z.X. Pi, W.H. Xu, J.H. Liu, Sens. Actuators B 99 (2004) 444–450.
[10] R.S. Niranjan, Y.K. Hwang, D.K. Kim, S.H. Jhung, J.S. Chang, L.S. Mulla, Mater. Chem. Phys. 92 (2005) 384–388.
[11] G.X. Wang, X.L. Gou, J. Horvat, J. Park, J. Phys. Chem. C 112 (2008) 15220–15225.
[12] X.H. Li, G.Y. Chen, L.B. Yang, Z. Jin, J.H. Liu, Adv. Funct. Mater. 20 (2010) 2815–2824.
[13] S.K. Kansal, M. Singh, D. Sud, J. Hazard. Mater. 153 (2008) 412–417.
[14] E. Vigil, F.A. Fernandez-Lima, J.A. Ayllon, E. Pedrero, I. Zumeta, B. Gonzalez, L. Curbelo, H.D. Fonseca-Filho, M.E.H. Maia-Costa, C. Domingo, M. Behar, F.C. Zawislak, Microporous Mesoporous Mater. 109 (2008) 560–566.
[15] A.I. Martinez, D.R. Acosta, G. Cedillo, Thin Solid Films 490 (2005) 118–123.

[16] M. Radecka, B. Lyson, M. Lubecka, A. Czapla, K. Zakrzewska, Acta Phys. Pol. A 117 (2010) 415–419.
[17] Z.Q. Cai, Q.H. Shen, J.W. Gao, H. Yang, J. Inorg. Mater. 22 (2007) 733–736.
[18] Z.Y. Liu, D.D. Sun, P. Guo, J.O. Leckie, Nano Lett. 7 (2007) 1081–1085.
[19] J.C. Zhang, Q. Li, W.L. Cao, J. Mater. Sci. Technol. 21 (2005) 191–195.
[20] Y. Zhao, J. Liu, L.Y. Shi, S.A. Yuan, J.H. Fang, Z.Y. Wang, M.H. Zhang, Appl. Catal. B: Environ. 100 (2010) 68–76.
[21] C.L. Chen, A. Ogino, X.K. Wang, M. Nagatsu, Appl. Phys. Lett. 96 (2010) 131504.
[22] B. Gehl, A. Fromsdorf, V. Aleksandrovic, T. Schmidt, A. Pretorius, J.I. Flege, S. Bernstorff, A. Rosenauer, J. Falta, H. Weller, M. Baumer, Adv. Funct. Mater. 18 (2008) 2398–2410.
[23] X.Y. Yu, T. Luo, Y.X. Zhang, Y. Jia, B.J. Zhu, X.C. Fu, J.H. Liu, X.J. Huang, ACS Appl. Mater. Interfaces 3 (2011) 2585–2593.
[24] X.Y. Yu, Z.Q. Jiang, Y.D. Meng, Plasma Sci. Technol. 12 (2010) 87–91.
[25] X.Y. Yu, Z.Q. Jiang, Y.D. Meng, Plasma Sci. Technol. 12 (2010) 224–229.
[26] J.Y. Liu, T. Luo, S. Mouli, F.L. Meng, B. Sun, M.Q. Li, J.H. Liu, Chem. Commun. 46 (2010) 472–474.
[27] A.M. Sevcenco, W.S. Lu, Multidimens. Syst. Signal Process. 21 (2010) 213–229.
[28] Z.Q. Sun, Y.L. Wang, Neural Comput. Appl. 18 (2009) 417–422.
[29] M.W. Berry, M. Browne, A.N. Langville, V.P. Pauca, R.J. Plemmons, Comput. Stat. Data Anal. 52 (2007) 155–173.
[30] D.M. Smilgies, J. Appl. Crystallogr. 42 (2009) 1030–1034.
[31] I.P. Muthuselvam, R.N. Bhowmik, J. Phys. D: Appl. Phys. 43 (2010) 465002.
[32] S. Yasmin, S. Choudhury, M.A. Hakim, A.H. Bhuiyan, M.J. Rahman, J. Mater. Sci. Technol. 27 (2011) 759–763.
[33] J.Y. Yang, W.S. Li, H. Li, Y. Sun, R.F. Dou, C.M. Xiong, L. He, J.C. Nie, Appl. Phys. Lett. 95 (2009) 213105.
[34] N.L. Wu, S.Y. Wang, I.A. Rusakova, Science 285 (1999) 1375–1377.
[35] K.R. Hahn, A. Tricoli, G. Santarossa, A. Vargas, A. Baiker, Surf. Sci. 605 (2011) 1476–1482.
[36] C. Xu, J. Tamaki, N. Miura, N. Yamazoe, Sens. Actuators B 3 (1991) 147–155.
[37] A. Tricoli, M. Righettoni, A. Teleki, Angew. Chem. Int. Ed. 49 (2010) 7632–7659.